Biogeosciences
Open Access

Disparities between in situ and optically derived carbon biomass and growth rates of the prymnesiophyte *Phaeocystis globosa*

L. Peperzak[1,2], H. J. van der Woerd[1], and K. R. Timmermans[2]

[1]Institute for Environmental Studies (IVM), VU University Amsterdam, the Netherlands
[2]Royal Netherlands Institute for Sea Research/NIOZ, Department of Biological Oceanography, Texel, the Netherlands

Correspondence to: L. Peperzak (louis.peperzak@nioz.nl)

Abstract. The oceans play a pivotal role in the global carbon cycle. It is not practical to measure the global daily production of organic carbon, the product of phytoplankton standing stock and its growth rate using discrete oceanographic methods. Instead, optical proxies from Earth-orbiting satellites must be used. To test the accuracy of optically derived proxies of phytoplankton physiology and growth rate, hyperspectral reflectance data from the wax and wane of a *Phaeocystis* bloom in laboratory mesocosms were compared with standard ex situ data. Chlorophyll biomass could be estimated accurately from reflectance using specific chlorophyll absorption algorithms. However, the conversion of chlorophyll (Chl) to carbon (C) was obscured by the non-linear increase in C : Chl under nutrient-limited growth. Although C : Chl was inversely correlated ($r^2 = 0.88$) with the in situ fluorometric growth rate indicator Fv / Fm (Photosystem II quantum efficiency), none of them was linearly correlated to growth rate, constraining the accurate calculation of *Phaeocystis* growth or production rates. Unfortunately, the optical proxy φ_{ph} (quantum efficiency of fluorescence: the ratio of the number of fluoresced photons to the number of photons absorbed by the phytoplankton) did not show any correlation with *Phaeocystis* growth rate, and therefore it is concluded that φ_{ph} cannot be applied in the remotely sensed measurement of this species' carbon production rate.

1 Introduction

Approximately half of the global photosynthetic CO_2 to organic carbon conversion takes place in marine waters (Field et al., 1998). Unfortunately, global daily CO_2 fixation, the product of phytoplankton standing stock and growth rates cannot be measured directly for the world oceans. Phytoplankton biomass and growth rates can be assessed directly and accurately by standard oceanographic techniques, but these miss the spatial coverage of the optical instruments on-board Earth-orbiting satellites. On the other hand, optically derived estimates of phytoplankton biomass and growth rates are less accurate than shipboard data (Abbott and Letelier, 1999; Carder et al., 2003; Behrenfeld et al., 2005; Huot et al., 2005; Astoreca et al., 2009; Martinez-Vicente et al., 2013). Here we report, to our knowledge for the first time ever, on the simultaneous evaluation of standard oceanographic and state-of-the-art optical techniques for gauging both phytoplankton biomass and carbon growth rates.

In "standard" oceanographic measurements, carbon concentration, carbon fixation, chlorophyll and other photopigment concentrations are analyzed in discrete water samples (ex situ), as is the quantum efficiency of Photosystem II (Fv / Fm) that can be considered an indicator for phytoplankton growth rate (Kromkamp and Foster, 2003; Ly et al., 2014).

Optical estimates of the oceanic carbon concentration for growth rate estimations can be made from the particulate backscatter coefficient (b_{bp}; Behrenfeld et al., 2005), but this coefficient is non-specific for phytoplankton or valid only for low chlorophyll *a* concentrations (Martinez-Vicente et al., 2013). Alternatively, the phytoplankton-specific chlorophyll concentration can be estimated from water-leaving radiance as absorbance (Carder et al., 2003). However, the carbon to chlorophyll ratio (C : Chl) that is then needed to convert chlorophyll into carbon is not a constant (Sathyendranath et al., 2009).

A second optical growth rate proxy is the phytoplankton-specific red chlorophyll fluorescence relative to absorbance (φ_{ph}). By definition this "quantum efficiency of fluorescence" is the ratio of the number of fluoresced photons to the number of photons absorbed by the phytoplankton, i.e. by all cellular photopigments (Abbott and Letelier, 1999; Huot et al., 2005). According to Falkowski and Kolber (Falkowski and Kolber, 1995), the quantum efficiency of photosynthesis varies inversely to the quantum efficiency of fluorescence. If the production of chlorophyll stops under nutrient limitation, it is expected that C : Chl, fluorescence and φ_{ph} will increase (Kiefer, 1973; Falkowski et al., 1992; Behrenfeld et al., 2009).

Besides the lack of specificity, an inherent problem in the optical approach of organic carbon production is that estimates of carbon and chlorophyll are used in both biomass and growth rate proxies. Moreover, doubt has been raised whether the variability in remotely sensed phytoplankton physiology (φ_{ph}) is due to physiological changes in the phytoplankton or due to environmentally driven biases in algorithms needed to estimate φ_{ph} (Huot et al., 2005).

In order to study the variability in phytoplankton biomass, growth rate, absorbance and fluorescence under variable but fully controlled conditions, a mesocosm experiment was conducted where detailed "standard" oceanographic measurements were combined with close-sensing hyperspectral measurements. Phytoplankton dynamics in the mesocosms were experimentally manipulated under semi-natural conditions of temperature, irradiance and turbulence (Peperzak et al., 2011). The prymnesiophyte *Phaeocystis globosa*, a key species in marine primary production, was used as test organism (Wassmann et al., 1990; Smith et al., 1991; DiTullio et al., 2000; Vogt et al., 2012). Our ambition was to use the optical signature of *Phaeocystis globosa*, which can now be detected by the MERIS and MODIS satellites (Kurekin et al., 2014), to better understand the wax and wane of its blooms. This optical signature includes light absorption, light emission and the quantum efficiency of the phytoplankton. In particular we would like to know how optical proxies compare to standard oceanographic techniques for estimating primary production, because this is still one of the key questions in ocean color research (Cullen and Lewis, 1995; Saba et al., 2010; Huot et al., 2013, 2005; Behrenfeld et al., 2009).

2 Methods

2.1 Experimental

The flagellate, non-colony-forming strain Pg6-I of *Phaeocystis globosa* ("*Phaeocystis*") was inoculated in two duplicate 140 L mesocosms filled with 0.2 µm of filtered Atlantic Ocean water poor in organic and inorganic nutrients that had been diluted with Milli-Q™ water to a salinity of 34 g kg^{-1}. A detailed description of the mesocosms is given in Peperzak

et al. (2011). Temperature during *Phaeocystis* growth was kept at 15 °C. Irradiance was provided in a semi-sinusoidal light–dark (16 : 8 h) cycle with a maximum surface PAR of 41 W m^{-2} in mesocosm 1 and 45 W m^{-2} in mesocosm 2. Turbulence of the water was provided by pumping surface water to the bottom of the mesocosm at a turnover rate of 1 h. The water was enriched with macronutrients to 30 µM NO$_3^-$, 6.3 µM PO$_4^{3-}$, and trace metals and vitamin B1 (Peperzak et al., 2011). On day 8 of the experiment, when cells were in the stationary growth phase, mesocosm 1 received enrichment with the initial nutrient concentrations to examine the effect of alleviation of nitrogen limitation on the physiological and optical properties of *Phaeocystis*.

2.2 Sampling

Water samples were taken in the middle of the light period (13:00, all times listed in CET) to measure salinity; pH; cell abundance; dissolved inorganic nitrogen (DIN); soluble reactive phosphorus (SRP); HPLC (high-performance liquid chromatography) pigments including chlorophyll *a* (Chl *a*), chlorophyll *c*2 and *c*3 (summed as Chl *c*) and carotenoids; particulate organic carbon (POC) and nitrogen (PON), and PAM-derived (Walz, Water PAM™) Photosystem II quantum efficiency (Fv / Fm) on dark-adapted (> 20 min) samples. A detailed description of the analyses is provided elsewhere (Peperzak et al., 2011). See Table 1 for a list of measured and derived variables.

Surface irradiance (W m^{-2} nm^{-1}), used to convert radiance (W m^{-2} nm^{-1} sr^{-1}) to reflectance (R, sr^{-1}), was measured prior to and after the experiment. In addition, phytoplankton absorption was measured daily at 13:00 using a 0.55 L integrating cavity absorption meter (ICAM; *a*-sphere™, HOBI Labs, Tucson, AZ, USA). ICAM absorption data (a_{ph}, m^{-1}) were blank-corrected daily by subtracting the absorption of filtered seawater, then divided by chlorophyll *a* or *c* concentrations to obtain the chlorophyll-specific absorption coefficients (a_{Chl}^*, m^2 (mg chlorophyll)$^{-1}$) in both the exponential and the stationary *Phaeocystis* growth phase. *Phaeocystis* spectra of a_{Chl}^*, together with reflectance data, were used to determine the appropriate wavelengths in algorithms for the estimation of chlorophyll *a* (*c*) absorption from reflectance spectra. Details of the ICAM absorption, irradiance and radiance measurements are provided elsewhere (Peperzak et al., 2011).

2.3 Mesocosms, absorption and fluorescence algorithms

The mesocosm description and analysis of the spectra is based on the methodological paper of Peperzak et al. (2011), which contains an extensive description of the experiment, measurements, and validation of the analysis of the absorption and fluorescence signals. The mesocosm tank, height 0.75 m, diameter 0.5 m and water volume 0.14 m^3 was made

Table 1. List of used variables, measurements and computations.

Symbol	Description	Measurement or computation	Units
a_{ph}	Phytoplankton (total pigment) absorption coefficient	Integrating cavity absorption meter, from 400 to 672 nm	m^{-1}
$a_{Chl\ a\ (c)}$	Chlorophyll a or c absorption coefficient	ARP (-4λ)(-Chl a/c) 4-wavelength algorithm from reflectance spectrum (Eq. 2)	m^{-1}
a_{Chl}	Total chlorophyll absorption coefficient	$a_{Chl\ a} + a_{Chl\ c}$	m^{-1}
$a^*_{Chl\ a\ (c)}$	Chlorophyll a- or c-specific absorption coefficient	a_{ph}/Chl a (at 428 or 674 nm) or a_{ph}/Chl c (at 466 nm) (Table 2)	m^{-2} (mg Chl)$^{-1}$
C : Chl (a)	Carbon to chlorophyll (a) ratio	POC / Chl or POC / Chl a	$g\,g^{-1}$
C : N	Carbon to nitrogen ratio	POC / PON	$mol\,mol^{-1}$
Carotenoids	Sum of fucoxanthin, diatoxanthin, diadinoxanthin, β,ε- and β,β-carotene	HPLC	$\mu g\,L^{-1}$
C : cell	Carbon content per cell	POC / N_t	$pg\,cell^{-1}$
Carots : Chl	Carotenoids to chlorophyll ratio	Carots / Chl	Unitless
Chl a	Chlorophyll a	HPLC	$\mu g\,L^{-1}$
Chl c	Chlorophyll c	HPLC	$\mu g\,L^{-1}$
Chl	Sum of Chl a and Chl c	HPLC	$\mu g\,L^{-1}$
Chl $a(c)$: cell	Chl a (c) content per cell	Chl a (c)/N_t	$pg\,cell^{-1}$
DIN	Dissolved inorganic nitrogen	Continuous flow chemistry	$\mu mol\,L^{-1}$
F	Chlorophyll a fluorescence	Fluorescence emission	$\mu mol\ photons\,m^{-2}\,s^{-1}$
F_0	Dark-adapted chlorophyll fluorescence	Pulse amplitude modulation fluorometer	Unitless
F_v/F_m	Photosystem II quantum efficiency	Pulse amplitude modulation fluorometer	Unitless
$N_{t\ (t+1)}$	Cell concentration on day t ($t+1$)	Flow cytometer	$cells\,\mu L^{-1}$
N : cell	Nitrogen content per cell	PON / N_t	$pg\,cell^{-1}$
PFR	Potential fluorescence radiation	Irradiance (400–672 nm) absorption by phytoplankton	$\mu mol\ photons\,m^{-2}\,s^{-1}$
POC	Particulate organic carbon	Mass spectrometer	$\mu g\,L^{-1}$
PON	Particulate organic nitrogen	Mass spectrometer	$\mu g\,L^{-1}$
R	Reflectance	Water-leaving radiance/surface irradiance	sr^{-1}
SRP	Soluble reactive phosphate	Continuous flow chemistry	$\mu mol\,L^{-1}$
φ_{ph}	Quantum efficiency of fluorescence	(F/PFR) x 100 %	%
μ	Cell specific growth rate between day$_t$ and day$_{t+1}$	$\ln (N_{t+1}/N_t)/$ (day$_{t+1}$ − day$_t$)	day^{-1}
μ POC	Carbon specific growth rate between day$_t$ and day$_{t+1}$	$\ln (POC_{t+1}/POC_t)/$ (day$_{t+1}$ − day$_t$)	day^{-1}

of black high-density polyethylene and mounted in a black metal frame made of 30 mm square aluminum painted black (Fig. 1). To avoid light reflection from the walls, the interior of the tank was sand-blasted. The contents was mixed by pumping water at a turnover rate of 1 h from 0.05 m below the water surface (-0.05 m) to 0.10 m above the bottom (-0.65 m). A total of 25 Solux™ MR16 halogen 4700 K "daylight" lamps of 50 W with a 24° beam spread were used in a 5×5 matrix in a black-painted box that was mounted in a frame at 0.70 m above the water surface. A variable light–dark cycle with a semi-sinusoidal illumination was made possible by timers controlling all lamps.

Prior to and after the experiments of two weeks, surface irradiance (E_0) was measured every 15 min for at least 24 h from 320 to 950 nm in 190 channels (W m^{-2} nm^{-1}) with a TriOS™ RAMSES-ACC-VIS hyperspectral cosine ir-

radiance sensor (TriOS, GmbH, Oldenburg, Germany) that was placed in the center of the mesocosm at the position of the water surface. During experiments the irradiance at the bottom (E_b) of the mesocosm (Fig. 1) was measured every 15 min with a similar TriOS™ hyperspectral cosine irradiance sensor. Water-leaving radiance (L_w) was measured every 15 min with a TriOS™ RAMSES-ACC-VIS hyperspectral radiance sensor (radiometer, 320–950 nm in 190 channels, W m^{-2} nm^{-1} sr^{-1}) at an angle of 50° nadir at 0.08 m above the water surface (Fig. 1). An integrating cavity absorption meter or ICAM (a-sphere spectrophotometer, HOBI Labs™, Tucson, AZ, USA) was used as an independent method to measure sample absorption (m^{-1}). This type of instrument is very accurate, also at low concentrations, without interference from particle scattering.
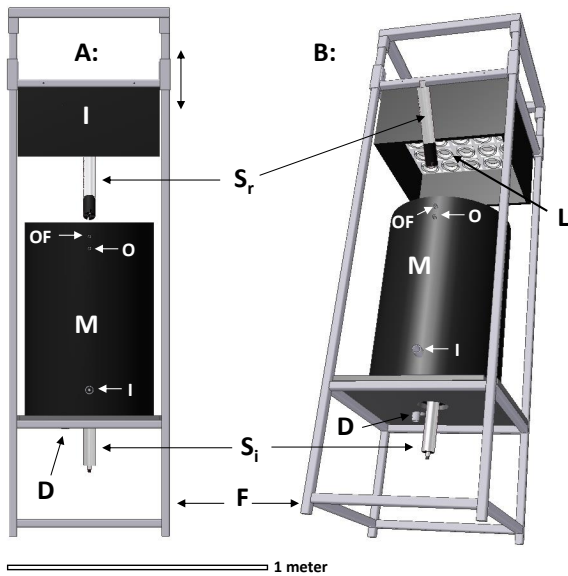
Figure 1. Schematic representation of the mesocosm system. A: side view; B: view from below. The mesocosm vessel (M, height 0.75 m, diameter 0.50 m) is placed inside a metal frame (F) that also holds the illumination box (I). The illumination box contains 25 Solux™ lamps (L) and is height-adjustable. Two hyperspectral sensors were installed: one for bottom irradiance (S_i) and one for water-leaving radiance (S_r). Water was pumped round through an outlet at -0.10 m (O) and an inlet at $+0.10$ m from the bottom. An overflow (OF) at -0.05 m was used to keep the water level constant. The mesocosm is emptied with a drain (D) in the bottom. For clarity, the construction holding the radiance sensor (S_r) and the electrical wiring, tubing, valves and pump are not shown.

Based on the averaged spectra from the middle of the light period (13:00–14:00), four optical properties were derived: (1) the total number of photons absorbed by phytoplankton, (2) the total number of photons emitted by fluorescence, and (3) the chlorophyll c and (4) chlorophyll a concentration. The fifth quantity, the phytoplankton quantum efficiency (φ_{ph}), is defined as the ratio of moles of photons emitted as fluorescence divided by the moles of photons absorbed by the pigments and is therefore the ratio of property 2 over 1.

From a comparison of the irradiance sensor at the bottom of each mesocosm with the known irradiance at the water surface, the wavelength-dependent attenuation in the mesocosm was derived. This attenuation was corrected for the (small) effects of pure water and scattering effects at the mesocosm wall, and the total number of absorbed photons was calculated as the absorption times the illumination at each wavelength and integrated over the interval 400–672 nm. The stricter upper limit of 672 nm to the potential fluorescence radiation (PFR) is based on a central fluorescence emission at 682 nm and a Stokes shift of 10 nm that determined the minimum extra energy needed for the excitation of a chlorophyll molecule. The typical available PFR just below the wa-

ter surface is 138 µmol photons m^{-2} s^{-1} for mesocosm 1, and slightly higher for mesocosm 2 (151 µmol photons m^{-2} s^{-1}).

The classic fluorescence line height (FLH) algorithm (Abbott and Letelier, 1999) was applied on the remote sensing reflectance spectra (R), calculated as the ratio of the radiance spectra collected above water (S_r, Fig. 1) divided by the illumination irradiance.

$$\text{FLH} = R_{max} - R_{base}(\text{sr}^{-1}), \tag{1a}$$

with $R_{base} = R_{b1} + (\lambda_{max} - \lambda_{b1}) \cdot ((R_{b1} - R_{b2})/(\lambda_{b1} - \lambda_{b2}))(\text{sr}^{-1}).$ (1b)

R_{max} is at the fluorescence peak ($\lambda = 682$ nm) in the mesocosm reflectance spectra and R_{base} is the baseline reflectance value at R_{max}, calculated linearly from the reflectance between R_{b1} and R_{b2}, with $b_1 = 650$ nm and $b_2 = 710$ nm. In order to derive the number of emitted photons in the mesocosm, the FLH was first multiplied by the irradiance spectrum to obtain a baseline corrected radiance above water at 682 nm (W m^{-2} nm^{-1} sr^{-1}). Then the signal was converted to photons and integrated over 4π sr (assuming isotropic emission) and integrated over the spectral range (650–710 nm), assuming a Gaussian distribution with a full width at half maximum (FWHM) of 25 nm. Subsequently, the emission was corrected for the water–air transition and the internal absorption in the mesocosm before it reaches the radiance sensor by water (0.43 m^{-1} at 682 nm) and self-absorption by the phytoplankton (Huot et al., 2005). We refer the reader to the publication of Peperzak et al. (2011) for a more extensive description and validation of this conversion.

The chlorophyll c concentration was calculated from reflectance (R) using a four-wavelength (at $\lambda = 450, 466, 480$ and 700 nm) absorption algorithm (ARP-4$\lambda_{\text{Chl } c}$) that was developed and positively applied by Astoreca et al. (2009) to detect *Phaeocystis* in the North Sea:

$$a_{\text{Chl } c} = a_{w,\,700} \cdot R_{700} \cdot (1/R_{466} - (1/R_{450})^{(1-w)} \cdot (1/R_{480})^{w})(\text{m}^{-1}), \tag{2a}$$

with the absorption by pure water

$$a_{w,\,700} = 0.572\,\text{m}^{-1}(15\,°\text{C}) \quad \text{(Buiteveld et al., 1994)}. \tag{2b}$$

The weight (w) is determined by the position of the Chl c absorption maximum (466 nm) relative to the two reference (baseline) wavelengths (450 and 480 nm):
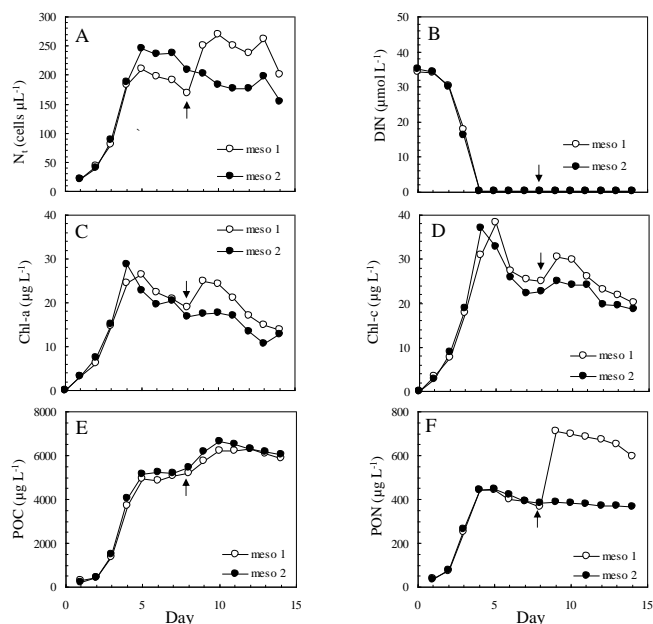
$$w = (\lambda_{466,\,\text{Chl } c} - \lambda_{450})/(\lambda_{480} - \lambda_{450}) = 0.53. \tag{2c}$$

A comparable absorption algorithm (ARP-4$\lambda_{\text{Chl } a}$) for chlorophyll a was derived after choosing the appropriate wavelengths, including the Chl a absorption maximum (438 nm):

$$a_{\text{Chl } a} = a_{w,\,700} \cdot R_{700} \cdot (1/R_{438} - (1/R_{425})^{(1-w)} \cdot (1/R_{450})^{w})(\text{m}^{-1}), \tag{3a}$$

with water absorption given by Eq. (1b) and the weight (w) by

$$w = (\lambda_{438,\,\text{Chl } a} - \lambda_{425})/(\lambda_{450} - \lambda_{425}) = 0.52. \tag{3b}$$

Figure 2. (a–f) *Phaeocystis*, nutrient and carbon dynamics in two mesocosms (meso 1, meso 2) in time. **(a)** Cell abundances (cells µL^{-1}), **(b)** dissolved inorganic nitrogen (DIN, µmol L^{-1}), **(c)** chlorophyll *a* (Chl *a*, µg L^{-1}), **(d)** chlorophyll *c* (Chl *c*, µg L^{-1}), **(e)** particulate organic carbon (POC, µg L^{-1}), **(f)** particulate organic nitrogen (PON, µg L^{-1}). The arrow indicates the nutrient addition to mesocosm 1 after sampling on day 8.

2.4 Statistics

To test the null hypothesis that there is no difference between means of variables measured in the two mesocosms, two-sample *t* tests were performed in SYSTAT™ version 12. Linear regression equations were calculated in SYSTAT™ or Excel™ 2003. The 95 % confidence intervals (±95 % CI) around a variable mean (*m*) were calculated from a *t* distribution using *n* observations (days), *n*–1 degrees of freedom (df) and the standard deviation of the mean SD as $m \pm 95\% \, CI = m \pm t \, (0.05; n-1) \times SD/\sqrt{n}$. The standard error (i.e., $SD/\sqrt{n}$) provided in linear regression by SYSTAT™ was used to calculate 95 % confidence intervals of regression slopes.

3 Results

3.1 Phytoplankton dynamics (ex situ observations)

Inoculation of the mesocosms was followed by a 3-day exponential increase in *Phaeocystis* cell abundance and Chl *a*, Chl *c*, POC and PON concentrations (Fig. 2a, c–f). Compared to mesocosm 1, the higher surface irradiance in mesocosm 2 led to 17 % more cells on day 5, when the stationary growth phase was reached in both mesocosms due to nitrogen limitation (Fig. 2b). In both mesocosms, cell abundances
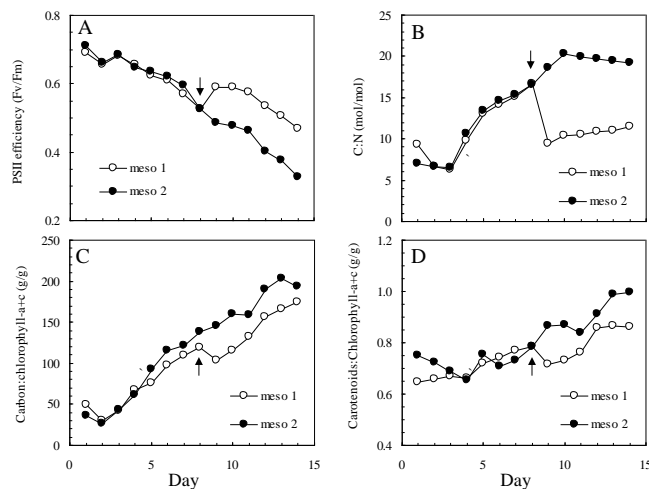

Figure 3. (a–d) *Phaeocystis* physiology and pigment ratios in two mesocosms in time. **(a)** Photosystem II efficiency (Fv / Fm), **(b)** carbon to nitrogen ratio (C : N, mol mol^{-1}), **(c)** carbon to chlorophyll *a* + *c* ratio (C : Chl *a* + *c*, g g^{-1}), and **(d)** carotenoids to chlorophyll *a* + *c* ratio (g g^{-1}). The arrow indicates the nutrient addition to mesocosm 1 after sampling on day 8.

in the stationary growth phase decreased at an average rate of $-0.07 \, \text{d}^{-1}$. The 30 µM nitrate in the nutrient spike added to mesocosm 1 on day 8 was already depleted by *Phaeocystis* on day 9 (Fig. 2b) and incorporated as PON (Fig. 2f). In addition, *Phaeocystis* cells and Chl *a* and Chl *c* concentrations increased after the nutrient spike (Fig. 2a, c–d). In a separate experiment (no data shown), in which a mesocosm 2 water sample on day 10 was spiked with only nitrate, the resumption of cell growth and an increase in Fv / Fm confirmed that nitrogen was the limiting element.

3.2 Physiology and pigment composition (ex situ observations)

After the depletion of DIN on day 4, Fv / Fm declined in both mesocosms (Fig. 3a), while the C : Chl ratios increased (Fig. 3c). The nutrient spike on day 8 in mesocosm 1 caused a temporary increase in Fv / Fm (Fig. 3a) and led to significantly lower C : N ($t = -25.2$, df = 5, $p < 0.001$) and C : Chl ratios ($t = -8.5$, df = 5, $p < 0.001$) in mesocosm 1 relative to mesocosm 2 (Fig. 3b, c). The difference in carotenoids : Chl between mesocosm 1 and 2 (Fig. 3d) from day 9 onwards was also significant ($t = -6.8$, df = 5, $p < 0.01$). Thus, the nutrient spike on day 8 caused a shift in Fv / Fm, C : N, C : Chl and carotenoids : Chl (Fig. 3).
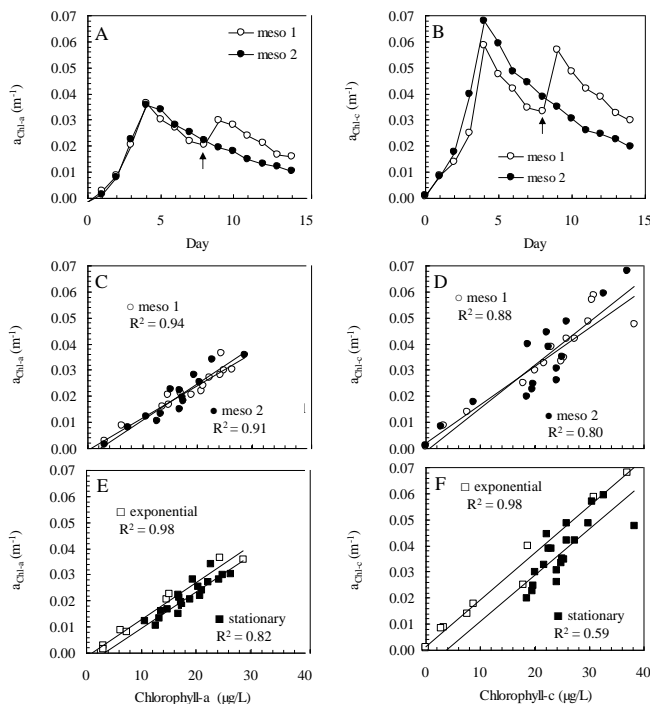
Figure 4. (a–f) Absorption characteristics in *Phaeocystis*. **(a–b)** Temporal development (days) of absorption by chlorophyll *a* (**a**, $a_{Chl\,a}$, m^{-1}) and *c* (**b**, $a_{Chl\,c}$, m^{-1}) calculated from reflectance spectra in both mesocosms. **(c–f)** Linear regression of absorption on chlorophyll *a* and *c* (m^{-1}) against Chl *a* and Chl *c* concentrations (µg L^{-1}) was performed separately for both mesocosms **(c, d)** and for exponential and stationary growth phases **(e, f)**.

3.3 Absorption and fluorescence (optical observations)

3.3.1 ICAM absorption

The ICAM absorption spectra of mesocosm water samples contained three major peaks: at 438 (Chl *a*), 466 (Chl *c*) and 674 nm (Chl *a*). In the exponential growth phase, a^*_{Chl} was lower than in the stationary growth phase, due to the increase in carotenoids after nitrogen was depleted (Fig. 3d). These differences in a^*_{Chl} between the exponential and stationary growth phase were significant at 438 and 466 nm, but not at 674 nm (Table 2).

3.3.2 Reflectance absorption

The specific chlorophyll *a* and *c* absorption ($a_{Chl\,a}$ and $a_{Chl\,c}$) computed from reflectance spectra (Fig. 4a–b) closely resembled the development of *Phaeocystis* cell abundance and Chl *a* and *c* concentrations (Fig. 2a, c–d). In both mesocosms, total Chl absorption, $a_{Chl\,a\,(c)}$ correlated well with HPLC-measured Chl *a* and Chl *c* concentrations (Fig. 4c–d) and the regression slopes of the two variables in the mesocosms were not significantly different (Table 3). When the data of both mesocosms were split by growth phase,
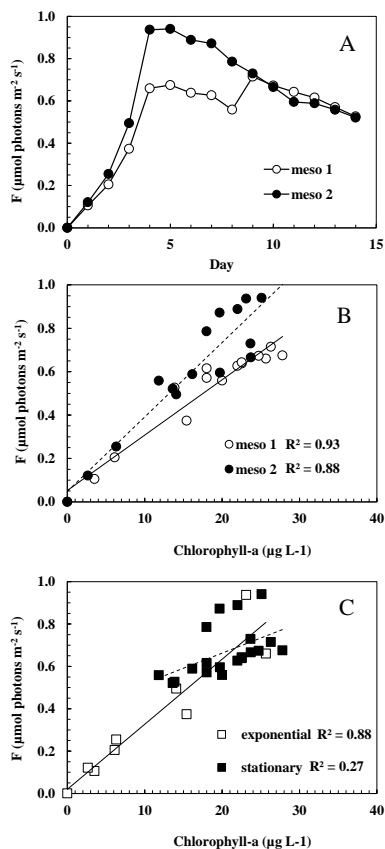
Figure 5. (a–c) Fluorescence emission. **(a)** Daily development of the fluorescence emission near 682 nm (*F*, µmol photons m^{-2} s^{-1}) calculated from reflectance spectra, **(b)** linear regression of fluorescence (*F*, µmol photons m^{-2} s^{-1}) on chlorophyll *a* (µg L^{-1}) for both mesocosms separately, and **(c)** for both exponential and stationary growth phases.

the exponential-phase (day 1 to 4) regression equations accurately (both $r^2 = 0.98$) estimated both Chl *a* and Chl *c* (Fig. 4e–f). The stationary-phase (day 5 to 14) regression intercepts between $a_{Chl\,a\,(c)}$ and Chl *a* and Chl *c* concentrations were lower than in the exponential growth phase (Fig. 4e–f), although not significantly (Table 3). This means that application of the regression equations combining both growth phases (Table 3) will lead to small underestimations of Chl *a* and Chl *c* concentrations in the exponential growth phase, and small overestimations of Chl *a* and Chl *c* concentrations in the stationary phase (Fig. 4e–f).

3.3.3 Fluorescence

Fluorescence emission estimated from the water-leaving radiance (Fig. 5a) resembled *Phaeocystis* cell dynamics (Fig. 2a) and was well correlated with Chl *a* (Fig. 5b; overall $r^2 = 0.81$, Table 4). When the data of both mesocosms were split by growth phase, the stationary-phase (day 5 to 14) regression slope and intercept were significantly different from

Table 2. *Phaeocystis* chlorophyll-specific absorption coefficients peaks in m^2 (mg Chl)$^{-1}$ during exponential and stationary growth. Listed are averages ±95 % confidence intervals.

Mesocosm number	N	Day	Growth phase	$a^*_{\text{Chl }a}$ (438 nm)	$a^*_{\text{Chl }c}$ (466 nm)	$a^*_{\text{Chl }a}$ (674 nm)
1 + 2	6	2–4	Exponential	0.053 ± 0.005	0.044 ± 0.005	0.026 ± 0.003
1	4	10–13	Stationary	0.081 ± 0.012	0.059 ± 0.003	0.033 ± 0.004
2	4	10–13	Stationary	0.091 ± 0.015	0.058 ± 0.004	0.036 ± 0.005

Table 3. Linear regression equations of *Phaeocystis* absorption on HPLC-measured chlorophyll a and c concentrations. Absorption was calculated with the ARP-4λ-Chl a and ARP-4λ-Chl c algorithms (Eq. 1). Regressions were made for the mesocosms separately, for exponential (day 0–4) and stationary (day 5–14) growth phases. Indicated are slope and intercepts ± 95 % confidence interval.

		N	Slope ($\times 10^{-3}$)	Intercept ($\times 10^{-3}$)	R^2
Chl a	Mesocosm 1	15	1.2 ± 0.1	−0.6 ± 2.8	0.94
Chl a	Mesocosm 2	15	1.4 ± 0.2	−3.1 ± 3.5	0.91
Chl a	Exponential	10	1.4 ± 0.1	−1.3 ± 1.8	0.98
Chl a	Stationary	20	1.4 ± 0.3	−4.4 ± 5.0	0.82
Chl a	Stationary*	19	1.4 ± 0.3	−4.6 ± 5.4	0.80
Chl a	Combined	30	1.3 ± 0.1	−1.8 ± 2.0	0.92
Chl c	Mesocosm 1	15	1.5 ± 0.2	2.0 ± 6.2	0.88
Chl c	Mesocosm 2	15	1.7 ± 0.4	−1.0 ± 8.6	0.80
Chl c	Exponential	10	1.8 ± 0.2	1.3 ± 2.9	0.98
Chl c	Stationary	20	1.8 ± 0.6	−6.7 ± 14.7	0.59
Chl c	Stationary*	19	1.6 ± 0.6	−4.0 ± 14.6	0.56
Chl c	Combined	30	1.6 ± 0.2	0.6 ± 4.9	0.84

* Day 9 of mesocosm 1 excluded (1 day after nutrient spike).

those in the exponential phase (day 1 to 4; Fig. 5c, Table 4). This means that, according to expectation, nutrient-stressed cells in the stationary growth phase have higher fluorescence intensity per unit chlorophyll.

3.4 Fluorescence quantum efficiency (optical observations)

The fluorescence efficiency (φ_{ph}), calculated as moles of photons emitted as fluorescence divided by the moles of photons absorbed by the phytoplankton pigments, increased during exponential growth, stabilized from day 5 to 8 and then decreased (Fig. 6). No apparent change in φ_{ph} was observed in response to the nutrient spike on day 8 to mesocosm 1.

3.5 Carbon growth rate and proxy comparison

In order to relate dynamics in light absorption and fluorescence to *Phaeocystis* physiology in the different growth phases, the dynamics of carbon growth rate (μ_{POC}) was compared to Fv / Fm, C : Chl and φ_{ph} (Fig. 7a–c). Because the cellular Chl c content of *Phaeocystis* is about the same as the cellular Chl a content (Fig. 4c, d) and total chlorophyll (Chl) was linearly correlated to Chl a (Chl = 2.28 × Chl a,

$r^2 = 0.99$), C : Chl was used rather than C : Chl a and C : Chl c separately.

The proxy comparison showed hyperbolic relations of μ_{POC} with C : Chl and Fv / Fm with highly variable values at $\mu_{\text{POC}} \sim 0.0\,\text{d}^{-1}$ (Fig. 7a–b). As could be expected from Fig. 7a and b, Fv / Fm was inversely linearly correlated to C : Chl ($r^2 = 0.88$). The good correlation implies that, under the present experimental conditions, Fv / Fm and C : Chl, as measured either in water samples or derived from water-leaving radiance, are directly comparable physiological proxies.
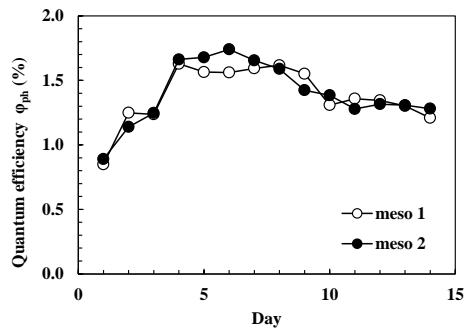
Fluorescence quantum efficiency did not show any correlation with growth rate (Fig. 7c). It appears that φ_{ph} is a poor proxy for *Phaeocystis* carbon production in both mesocosms.

4 Discussion

The aim of the mesocosm experiments was to investigate a relation between optical remote sensing and "standard" oceanographic measurements of phytoplankton physiology during different growth phases (here: nitrogen-controlled growth) of *Phaeocystis* and to infer possible implications for estimates of primary productivity. The standard physiological and reflectance measurements, in combination with

Table 4. Linear regression equations of *Phaeocystis* fluorescence on HPLC-measured chlorophyll *a* concentrations. Fluorescence was calculated with the FLH-H algorithm (Eq. 2). Regressions were made for the mesocosms separately, for exponential (day 0–4) and stationary (day 5–14) growth phases. Indicated are slopes and intercepts ±95 % confidence intervals.

|		N	Slope ($\times 10^{-2}$)	R^2
Chl *a*	Mesocosm 1	15	2.6 ± 0.4	0.93
Chl *a*	Mesocosm 2	15	3.4 ± 0.8	0.88
Chl *a*	Exponential	10	3.1 ± 0.8	0.88
Chl *a*	Stationary	20	1.4 ± 1.1	0.27
Chl *a*	Combined	30	2.9 ± 0.5	0.81

Figure 6. Development in time (days) of quantum efficiency φ_{ph} derived from total phytoplankton absorption and fluorescence in two mesocosms.

the effect of a nutrient spike to one mesocosm, proved that growth of *Phaeocystis* was indeed nitrogen-limited during the experiments. By measuring the in situ fluorescence (F) increase due to nitrogen limitation, and the increase in photons absorbed by phytoplankton (PFR), an optical estimate of the quantum efficiency of fluorescence φ_{ph} (i.e., F / PFR) could be made. It is shown that of the physiological diagnostics neither φ_{ph}, nor Photosystem II quantum efficiency (Fv / Fm) nor C : Chl are reliable estimators of *Phaeocystis* growth rates. This may have consequences for global carbon fixation estimates using remote sensing data assessing phytoplankton physiology.

4.1 Phytoplankton dynamics

Temperature, salinity, irradiance and pH were at or near values for optimum *Phaeocystis* growth (Peperzak, 2002). The exponential-phase growth rate ($\mu = 0.7 \, \mathrm{d}^{-1}$) and stationary-phase mortality rate ($d = -0.07 \, \mathrm{d}^{-1}$) were equal to the rates obtained in cultures of *P. globosa* strain Ph91 (Peperzak et al., 2000a, b). The carbon and photopigment contents of *Phaeocystis* in the mesocosms were comparable to published values, although cellular Chl *a* and Chl *c* content was relatively low (Table 5). On the other hand, the fucoxanthin to Chl *a* ratio was high, which is probably caused by
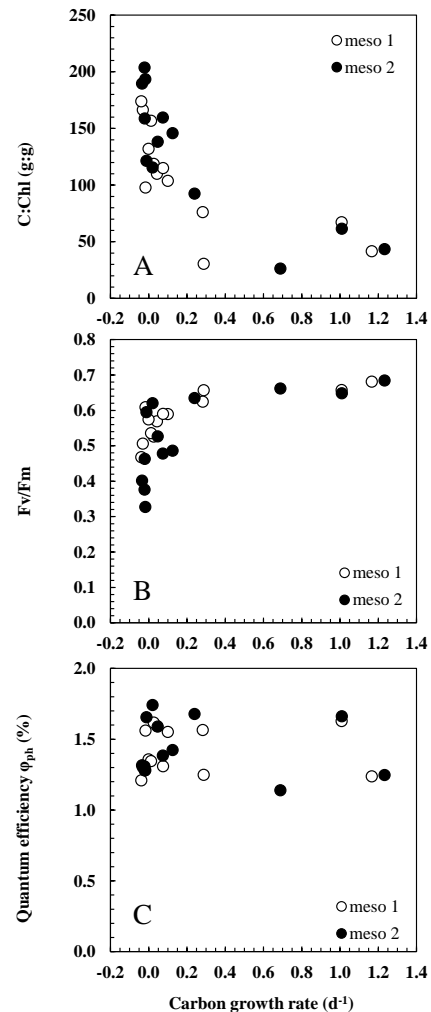
Figure 7. Three proxies for growth rate as a function of measured carbon growth rate (μ_{POC}, d^{-1}): **(a)** carbon to chlorophyll $a + c$ ratio (C : Chl $a + c$, $\mathrm{g \, g}^{-1}$), **(b)** Photosystem II efficiency (Fv / Fm) and **(c)** quantum efficiency (φ_{ph}, %). Data combined from both mesocosms.

(1) an adaptation to the low-irradiance environment where this flagellate can thrive (Peperzak, 1993; Seoane et al., 2009) and/or (2) the effect of nitrogen-limited growth on the carotenoids : Chl ratio (Fig. 3d). In mesocosm 2, *Phaeocystis* in the stationary phase reached a C : N of 20, which is equal to the subsistence quota of $0.05 \, \mathrm{mol \, N \, mol \, C}^{-1}$ in diatoms (Edwards et al., 2003). The rapid depletion of nitrate during the initial days of the experiment and the constant increase in C : N – combined with the decrease in C : N, resumption of cell growth and increase in Fv / Fm after the nutrient spike – convincingly showed that *Phaeocystis* was nitrogen-limited in the stationary phase.

The physiological indicator Fv / Fm declined when nitrogen had been depleted on day 4. In addition, C : Chl increased. Both indicators responded directly following the nutrient spike to the nitrogen-depleted *Phaeocystis* on day 8.

Table 5. Biochemical characteristics of *Phaeocystis* in the mesocosm compared to published data from cultures, unless otherwise indicated. Chl is the sum of chlorophyll *a* and *c*; Fuco: fucoxanthin.

Variable	Unit	Mesocosm	Published/field	Reference
Carbon content	pg cell^{-1}	10–40	11	(Rousseau et al., 1990)
Chlorophyll *a*	pg cell^{-1}	0.1–0.2	0.1–0.3[a]	(Buma et al., 1991)
			1.8[a]	
Chlorophyll *c*	pg cell^{-1}	0.1–0.2	0.3[a]	(Buma et al., 1991)
			0.8[a]	(Astoreca et al., 2009)
C : Chl *a*	g : g	60–500	16–400[b]	(Falkowski et al., 1985)
			65–111[c]	(Sathyendranath et al., 2009)
C : Chl	g : g	30–200	–	–
Chl *c* : Chl *a*	g : g	1.1–1.9	0.1–0.8[e]	(Buma et al., 1991)
			0.4	(Astoreca et al., 2009)
			0.4	(Seoane et al., 2009)
Fuco : Chl *a*	g : g	1.2–2.2	0.2–0.3[d]	(Astoreca et al., 2009)
			0.3–0.8[e]	(Buma et al., 1991)
			0.3–1.0[d]	(Seoane et al., 2009)

[a] For larger non-flagellated *Phaeocystis* cells. [b] Range of three species cultured at different irradiances. [c] C : Chl *a* for prymnesiophytes in field samples determined by regression analysis. [d] High value at low irradiance. [e] In Marsdiep during *Phaeocystis* blooms (Wadden Sea tidal inlet).

C : Chl was inversely linearly correlated with Fv / Fm, but carbon growth rate was not. This can be explained by the fact that both Fv / Fm and C : Chl declined continuously after nitrogen depletion while cell division immediately halted on day 5. As a consequence, Fv / Fm and C : Chl not only signal physiological change but are also indicative of the persistence of nitrogen depletion in *Phaeocystis*. A comparable conclusion was reached for the decline of Fv / Fm and the duration of nitrogen depletion in the diatom *Thalassiosira pseudonana* (Parkhill et al., 2001). On the other hand, under balanced growth conditions, i.e. steady-state nitrogen-limited growth, the value of Fv / Fm in *T. pseudonana* was high and comparable to the value in nutrient-replete cultures (Parkhill et al., 2001). In other words, the steady 10-day change after an abrupt nitrogen depletion shows that Fv / Fm and C : Chl are not good indicators of short-term nutrient-limited phytoplankton growth rates.

In the early stationary phase (day 4–8), the 10 % lower surface irradiance in mesocosm 1 led to a slightly lower (94 ± 21) but not significantly different C : Chl than in mesocosm 2 (106 ± 28). Comparable minor effects on cellular chlorophyll contents have been measured in *Phaeocystis* cultured at 10 and 100 µmol photons m^{-2} s^{-1} (Astoreca et al., 2009). The reduction of water column irradiance due to self-shading by increased chlorophyll concentrations during exponential growth would therefore have little effect on C : Chl. Far more important than the (relatively weak) effect of irradiance on C : Chl was the factor of 10 variability in C : Chl when *Phaeocystis* went from the exponential (C : Chl = 30) to the late stationary growth phase (C : Chl = 200, Fig. 3c and Table 5). This variability confirms that chlorophyll concentration is not a reliable indicator of phytoplankton biomass

(Behrenfeld et al., 2009; Kruskopf and Flynn, 2006), which has implications for the correct conversion of chlorophyll to carbon in chlorophyll-based primary production models (Cloern et al., 1995; Sathyendranath et al., 2009).

4.2 Pigments and absorption

Nitrogen depletion led to increases in carotenoid concentrations relative to chlorophyll. Comparable increases in light absorption under nitrogen limitation, due to increased carotenoid : Chl *a* ratios, have been observed in other phytoplankton species (Heath et al., 1990; Staehr et al., 2002). The increase in carotenoids : Chl ratio had a direct effect on the estimation of light absorption from the reflection spectra and ICAM measurements. The excellent correlations (Table 3) between $a_{\text{Chl } a}$ and $a_{\text{Chl } c}$ as well as Chl *a* and Chl *c* concentrations in the exponential phase (both $r^2 = 0.98$) were lower in the stationary phase ($0.59 < r^2 < 0.82$). Besides more variability in the stationary phase, a_{Chl} was lower than in the exponential phase due to interference by carotenoids in the reflection spectrum. This interference was more pronounced for $a_{\text{Chl } c}$ than for the $a_{\text{Chl } a}$ (Table 3), because the $a_{\text{Chl } c}$ algorithm employs wavelengths from 450 to 480 nm, where carotenoid absorption is more pronounced (Fujiki and Taguchi, 2002; Lubac et al., 2008).

The interference of carotenoids in the stationary phase will increase if total pigment absorption (a_{ph}) is measured instead of specific chlorophyll absorption. It is not surprising, therefore, that by using the ICAM data (400 to 672 nm) the correlation of absorption with Chl was lower ($r^2 = 0.74$) than when using the Chl *a*- and Chl *c*-specific algorithms. Carotenoid interference in the stationary phase also explains the limited apparent linearity of chlorophyll detection by

ICAM absorption to a maximum of approximately $50\,\mu g\,L^{-1}$ (Peperzak et al., 2011). At a high nitrogen-limited *Phaeocystis* biomass, the use of total absorption, including the carotenoids, leads to an overestimation of the chlorophyll concentration.

4.3 Fluorescence quantum efficiency

The optically measured fluorescence signal correlated well with the ex situ measured Chl a concentrations and, as expected, showed a relative fluorescence increase in the stationary phase. φ_{ph} in mesocosm 2 ranged by more than $100\,\%$, from ≈ 0.8 to $\approx 1.7\,\%$ (Fig. 6). Satellite estimates of φ_{ph} have a corresponding range, 0–$3\,\%$ (Huot et al., 2005; Behrenfeld et al., 2009). However, there was no correlation with μ (cell growth rate) or μ_{POC} (carbon growth rate, Fig. 7c), due to the effect of a changing carotenoids : Chl ratio as a result of nitrogen limitation. This suggests that, in order to relate growth conditions and fluorescence signal strength, new optical proxies should be developed for the photon absorption and emission by individual pigments (Fawley, 1989).

Even though φ_{ph} can be estimated using appropriate fluorescence and absorbance algorithms, its value is not a reliable indicator of actual nitrogen-controlled *Phaeocystis* growth rate. φ_{ph} is also a diagnostic for the duration of nitrogen depletion in *Phaeocystis*, which adds to the discussion on the physiological significance of Fv / Fm and C : Chl. For instance, under steady-state nitrogen-limited growth, the value of Fv / Fm in *T. pseudonana* is as high as the value in nutrient-replete cultures (Parkhill et al., 2001). As the present investigation was deemed to be exemplary of the phytoplankton dynamics during the wax and wane of a short-term bloom, i.e. a fast reduction from a high concentration of the limiting nutrient towards depletion, a real-world estimate of φ_{ph} might behave similarly to φ_{ph} in the mesocosms.

On the other hand, in oceanic waters the supply of the limiting nutrient may be low but relatively more constant, such as by aeolian deposition of iron or by continuous heterotrophic remineralization of organic material in the water column. For iron-limited phytoplankton growth, φ_{ph} derived from satellite data was elevated (Behrenfeld et al., 2009), so in $82\,\%$ of the oceanic regions with a low iron deposition rate, φ_{ph} appears to be a reliable remote sensing physiology proxy. This applicability of φ_{ph} corresponds with that of Fv / Fm as a good physiological proxy in iron-limitation studies (Timmermans et al., 2001, 2008). Iron limitation likely has a more pronounced effect on φ_{ph} than limitation of the major nutrients (N, P).

The present *Phaeocystis* study is an example of how experiments can contribute to validation of assumptions on optical data that are being made in the estimation of global carbon production. More experimental data are needed from phytoplankton species that differ in their pigment composition and in the effects of short- and long-term nutrient (N, P, Fe) limitation so that new optical proxies for phytoplankton physiology can be examined. Until these issues have been resolved we should be aware of the obscured view of phytoplankton physiology and hence marine primary production estimates using remote sensing.

References

Abbott, M. R. and Letelier, R. M.: Algorithm theoretical basis document chlorophyll fluorescence (MODIS product number 20), NASA, 1–42, 1999.

Astoreca, R., Rousseau, V., Ruddick, K., Knechciak, C., van Mol, B., Parent, J.-Y., and Lancelot, C.: Development and application of an algorithm for detecting *Phaeocystis globosa* blooms in the Case 2 Southern North Sea waters, J. Plankton Res., 31, 287–300, 2009.

Behrenfeld, M. J., Boss, E., Siegel, D. A., and Shea, D. M.: Carbon-based ocean productivity and phytoplankton physiology from space, Global Biochem. Cy., 19, GB1006, doi:10.1029/2004GB002299, 2005.

Behrenfeld, M. J., Westberry, T. K., Boss, E. S., O'Malley, R. T., Siegel, D. A., Wiggert, J. D., Franz, B. A., McClain, C. R., Feldman, G. C., Doney, S. C., Moore, J. K., Dall'Olmo, G., Milligan, A. J., Lima, I., and Mahowald, N.: Satellite-detected fluorescence reveals global physiology of ocean phytoplankton, Biogeosciences, 6, 779–794, doi:10.5194/bg-6-779-2009, 2009.

Buiteveld, H., Hakvoort, J. M. H., and Donze, M.: The optical properties of pure water, Ocean Optics XII, 174–183, 1994.

Buma, A. G. J., Bano, N., Veldhuis, M. J. W., and Kraay, G. W.: Comparison of the pigmentation of two strains of the prymnesiophyte *Phaeocystis* sp., Neth. J. Sea Res., 27, 173–182, 1991.

Carder, K. L., Chen, R., and Hawes, S.: Algorithm theoretical basis document: Instantaneous photosynthetically available radiation and absorbed radiation by phytoplankton, Version 7, NASA, 24, 1–24, 2003.

Cloern, J. E., Grenz, C., and Vidergar-Lucas, L.: An empirical model of the phytoplankton chlorophyll:carbon ratio-the conversion factor between productivity and growth rate, Limnol. Oceanogr., 40, 1313–1321, 1995.

Cullen, J. and Lewis, A. G.: Biological processes and optical measurements near the sea surface: Some issues relevant to remote sensing, J. Geophys. Res., 100, 13255–213266, 1995.

DiTullio, G. R., Grebmeier, J. M., Arrigo, K. R., Lizotte, M. P., Robinson, D. H., Leventer, A., Barry, J. P., VanWoert, M. L., and Dunbar, R. B.: Rapid and early export of *Phaeocystis antarctica* blooms in the Ross Sea, Antarctica, Nature, 404, 595–598, 2000.

Edwards, V. R., Tett, P., and Jones, K. J.: Changes in the yield of chlorophyll a from dissolved available inorganic nitrogen after an enrichment event - applications for predicting eutrophication in coastal waters, Cont. Shelf Res., 23, 1771–1785, 2003. 1992.

Falkowski, P. and Kolber, Z.: Variations in Chlorophyll Fluorescence Yields in Phytoplankton in the World Oceans, Aust. J. Plant Physiol., 22, 341–355, 1995.

Falkowski, P., Greene, R. M., and Geider, R.: Physiological limitations on phytoplankton productivity in the ocean, Oceanogr. Mar. Biol., 5, 84–91, 1992.

Falkowski, P. G., Dubinsky, Z., and Wyman, K.: Growth-irradiance relationships in phytoplankton, Limnol. Oceanogr., 30, 311–321, 1985.

Fawley, M. W.: A new form of chlorophyll *c* involved in light-harvesting, Plant. Physiol., 91, 727–732, 1989.

Field, C. B., Behrenfeld, M. J., Randerson, J. T., and Falkowski, P.: Primary production of the biosphere: integrating terrestrial and oceanic components, Science, 281, 237–240, 1998.

Fujiki, T. and Taguchi, S.: Variability in chlorophyll *a* specific absorption coefficient in marine phytoplankton as a function of cell size and irradiance, J. Plankton Res., 24, 859–874, 2002.

Heath, M. R., Richardson, K., and Kiørboe, T.: Optical assessment of phytoplankton nutrient depletion, J. Plankton Res., 12, 381–396, 1990.

Huot, Y., Brown, C. A., and Cullen, J. J.: New algorithms for MODIS sun-induced chlorophyll fluorescence and a comparison with present data products, Limnol. Oceanogr.-Methods, 3, 108–130, 2005.

Huot, Y., Franz, B. A., and Fradette, M.: Estimating variability in the quantum yield of Sun-induced chlorophyll fluorescence: A global analysis of oceanic waters, Remote Sens. Environ., 132, 238–253, 2013.

Kiefer, D. A.: Chlorophyll *a* fluorescence in marine centric diatoms: Responses of chloroplasts to light and nutrient stress, Mar. Biol., 23, 39–46, 1973.

Kromkamp, J. and Foster, R. M.: The use of variable fluorescence measurements in aquatic ecosystems: differences between multiple and single turnover measuring protocols and suggested terminology, Eur. J. Phycol., 38, 103–112, 2003.

Kruskopf, M. and Flynn, K. J.: Chlorophyll content and fluorescence responses cannot be used to gauge reliably phytoplankton biomass, nutrient status or growth rate, New Phytol., 169, 525–536, 2006.

Kurekin, A. A., Miller, P. I., and Van der Woerd, H. J.: Satellite discrimination of Karenia mikimotoi and Phaeocystis harmful algal blooms in European coastal waters: Merged classification of ocean colour data, Harmful Algae, 31, 163–176, doi:10.1016/j.hal.2013.11.003, 2014.

Lubac, B., Loisel, H., Guiselin, N., Astoreca, R., Artigas, L. F., and Meriaux, X.: Hyperspectral and multispectral ocean color inversions to detect *Phaeocystis globosa* blooms in coastal waters, J. Geophys. Res., 113, C06026, doi:10.1029/2007JC004451, 2008.

Ly, J., Philippart, C. J. M., and Kromkamp, J.: Phosphorus limitation during a phytoplankton spring bloom in the western Dutch Wadden Sea, J. Sea Res., 88, 109–120, doi:10.1016/j.seares.2013.12.010, 2014.

Martinez-Vicente, V., Dall'Olmo, G., Tarran, G., Boss, E., and Sathyendranath, S.: Optical backscattering is correlated with phytoplankton carbon across the Atlantic Ocean, Geophys. Res. Lett., 40, 1154–1158, doi:10.1002/grl.50252, 2013.

Parkhill, J.-P., Maillet, G., and Cullen, J. J.: Fluorescence-based maximal quantum yield for PSII as a diagnostic of nutrient stress, J. Phycol. , 37, 517–529, 2001.

Peperzak, L.: Daily irradiance governs growth rate and colony formation of Phaeocystis (Prymnesiophyceae), J. Plankton Res., 15, 809–821, 1993.

Peperzak, L.: The wax and wane of *Phaeocystis globosa* blooms, Rijksuniversiteit Groningen, The Netherlands, Groningen, 254 pp., 2002.

Peperzak, L., Timmermans, K. R., Wernand, M. R., Oosterhuis, S., and Van der Woerd, H. J.: A mesocosm tool to optically study phytoplankton dynamics, Limnol. Oceanogr.-Methods, 9, 232–244, 2011.

Peperzak, L., Duin, R. N. M., Colijn, F., and Gieskes, W. W. C.: Growth and mortality of flagellates and non-flagellate cells of Phaeocystis globosa (Prymnesiophyceae), J. Plankton Res., 22, 107–120, doi:10.1093/plankt/22.1.107, 2000a.

Peperzak, L., Gieskes, W. W. C., Duin, R. N. M., and Colijn, F.: The vitamin B requirement of *Phaeocystis globosa* (Prymnesiophyceae), J. Plankton Res., 22, 1529–1537, 2000b.

Rousseau, V., Mathot, S., and Lancelot, C.: Calculating carbon biomass of *Phaeocystis* sp. from microscopic observations, Mar. Biol., 107, 305–314, 1990.

Saba, V. S., Friedrichs, M. A. M., Carr, M. E., Antoine, D., Armstrong, R. A., Asanuma, I., Aumont, O., Bates, N. R., Behrenfeld, M. J., Bennington, V., Bopp, L., Bruggeman, J., Buitenhuis, E. T., Church, M. J., Ciotti, A. M., Doney, S. C., Dowell, M., Dunne, J., Dutkiewicz, S., Gregg, W., Hoepffner, N., Hyde, K. J. W., Ishizaka, J., Kameda, T., Karl, D. M., Lima, I., Lomas, M. W., Marra, J., McKinley, G. A., Mélin, F., Moore, J. K., Morel, A., O'Reilly, J., Salihoglu, B., Scardi, M., Smyth, T. J., Tang, S., Tjiputra, J., Uitz, J., Vichi, M., Waters, K., Westberry, T. K., and Yool, A.: Challenges of modeling depth-integrated marine primary productivity over multiple decades: A case study at BATS and HOT, Global Biochem. Cy., 24, 1–30, doi:10.1029/2009GB003655, 2010.

Sathyendranath, S., Stuart, V., Nair, A., Oka, K., Nakane, T., Bouman, H., Forget, M.-H., Maass, H., and Platt, T.: Carbon-to-chlorophyll ratio and growth rate of phytoplankton in the sea, Mar. Ecol. Prog. Ser., 383, 73–84, 2009.

Seoane, S., Zapata, M., and Orive, E.: Growth rates and pigment patterns of haptophytes isolated from estuarine waters, J. Sea Res., 62, 286–294, 2009.

Smith, W. O., Codispoti, L. A., Nelson, D. M., Manley, T., Buskey, E. J., Niebauer, H. J., and Cota, G. F.: Importance of *Phaeocystis* blooms in the high-latitude ocean carbon cycle, Nature, 352, 514–516, 1991.

Staehr, P. A., Henriksen, P., and Markager, S.: Photoacclimation of four marine phytoplankton species to irradiance and nutrient availability, Mar. Ecol. Prog. Ser., 238, 47–59, 2002.

Timmermans, K. R., Davey, M. S., van der Wagt, B., Snoek, J., Geider, R. J., Veldhuis, M. J. W., Gerringa, L. J. A., and De Baar, H. J. W.: Co-limitation by iron and light of *Chaeotoceros brevis, C.*

dichaeta and *C. calcitrans* (Bacillariophyceae), Mar. Ecol. Prog. Ser., 217, 287–297, 2001.

Timmermans, K. R., Veldhuis, M. J. W., Laan, P., and Brussaard, C. P. D.: Probing natural iron fertilization near the Kerguelen (Southern Ocean) using natural phytoplankton assemblages and diatom cultures, Deep-Sea-Res.-Pt. II. , 55, 693–705, 2008.

Vogt, M., O'Brien, C., Peloquin, J., Schoemann, V., Breton, E., Estrada, M., Gibson, J., Karentz, D., Van Leeuwe, M. A., Stefels, J., Widdicombe, C., and Peperzak, L.: Global marine plankton functional type biomass distributions: Phaeocystis spp., Earth Syst. Sci. Data, 4, 107–120, doi:10.5194/essd-4-107-2012, 2012.

Wassmann, P., Vernet, M., Mitchell, B. G., and Rey, F.: Mass sedimentation of *Phaeocystis pouchetii* in the Barents Sea, Mar. Ecol. Prog. Ser., 66, 183–195, 1990.